John von Neumann Institute for Computing

Thermodynamic and Transport Properties of Dense Quantum Coulomb Systems

M. Bonitz, V.S. Filinov

published in

NIC Symposium 2004, Proceedings,
Dietrich Wolf, Gernot Münster, Manfred Kremer (Editors),
John von Neumann Institute for Computing, Jülich,
NIC Series, Vol. **20**, ISBN 3-00-012372-5, pp. 443-452, 2003.

http://www.fz-juelich.de/nic-series/volume20

Thermodynamic and Transport Properties of Dense Quantum Coulomb Systems

M. Bonitz[1] **and V.S. Filinov**[2]

[1] Fachbereich Physik, Universität Rostock
18051 Rostock, Germany
E-mail: bonitz@uni-rostock.de

[2] Institute for High Energy Density, Russian Academy of Sciences
Izhorskay 13/19, Moscow 127412, Russia
E-mail: filinov@ok.ru

Strong correlations in quantum Coulomb systems (QCS) are attracting increasing interest in many fields ranging from dense plasmas and semiconductors to metal clusters and ultracold trapped ions. Examples are bound states in dense plasmas (atoms, molecules, clusters) and semiconductors (excitons, trions, biexcitons) or Coulomb crystals. We present first principle simulation results of these systems including path integral Monte Carlo simulations of the equilibrium behavior of dense hydrogen and electron-hole plasmas and molecular dynamics and quantum kinetic theory simulations of the nonequilibrium properties of QCS. These large-scale simulations became feasible due to the supercomputer power of the NIC Jülich. They have the advantage that much more accurate predictions of the behaviour of very complex CQS are now available.

1 Introduction

The family of Coulomb systems, i.e. many-body systems which are dominated by Coulomb interaction, has grown beyond convential plasmas in space or laboratory for many years, for an overview see e.g. Ref. 1, 2. They include also electron-hole plasmas in semiconductors, the electron gas in metals, charged particles confined in various traps or storage rings, charged complex or dust particles and also small few-particle clusters in mesoscopic quantum dots. Despite their different nature, all Coulomb systems have similar fundamental properties which are governed by two parameters: the strength of the Coulomb interaction (measured by the coupling parameters Γ and r_s) and the strength of quantum effects (degeneracy parameter χ). These parameters are determined by the ratio of characteristic energy and length scales[3,4]:

- *Length scales*:
  1.) $\bar{r}$ – the average interparticle distance, $\bar{r} \sim n^{-1/d}$ (n and d denote the density and dimensionality , $d = 1, 2, 3$, of the system respectively).
  2.) Λ – the quantum-mechanical extension of the particles. For free particles, $\Lambda = h/\sqrt{2\pi m k_B T}$ (DeBroglie wavelength), for bound particles Λ is given by the extension of the wave function.
  3.) a_B – the relevant Bohr radius $a_B = \frac{\epsilon}{e_a e_b}\frac{\hbar^2}{m_{ab}}$, with $m_{ab}^{-1} = m_a^{-1} + m_b^{-1}$.
- *Energy scales*:
  1.) $\langle K \rangle$ – the mean kinetic energy, in a classical system $\langle K \rangle_{cl} = \frac{d}{2} k_B T$, whereas in a highly degenerate Fermi system $\langle K \rangle_{qm} = \frac{3}{5} E_F$ (E_F denotes the Fermi energy);

2.) the mean Coulomb energy – for free particles: $\langle U_c \rangle_f = \frac{e_a e_b}{4\pi\epsilon} \frac{1}{\bar{r}}$, and for bound particles: $\langle U_c \rangle_B = \frac{e_a e_b}{4\pi\epsilon} \frac{1}{2a_B} \equiv E_R$ (Rydberg).

- The *degeneracy parameter* $\chi \equiv n\Lambda^d \sim (\Lambda/\bar{r})^d$ divides many-body systems into classical ($\chi < 1$) and quantum mechanical ones ($\chi \geq 1$).
- The *Coulomb coupling parameter* is the ratio $|\langle U_c \rangle|/\langle K \rangle$. For classical systems $\Gamma \equiv |\langle U_c \rangle|/k_B T$, whereas for quantum systems the role of Γ is taken over by $r_s \equiv \bar{r}/a_B \sim |\langle U_c \rangle|/E_F$.

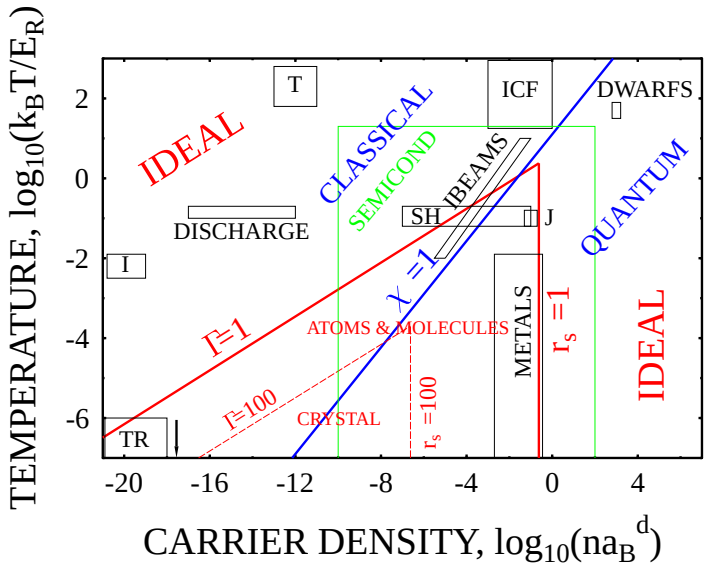

Figure 1. Universal density–temperature plane for Coulomb systems in equilibrium. The lines $\Gamma = 1$ and $r_s = 1$ enclose the region of strong Coulomb correlations, the lines $\Gamma = 100$ and $r_s = 100$ give an approximate boundary for Coulomb (Wigner) crystals. The line $\chi = 1$ separates classical (left) and quantum (right) systems. Abbreviations stand for CS in tokamaks (T), inertial confinement fusion (ICF), brown dwarf stars (DWARFS), Jupiter interior (J), ionosphere (I), shock wave plasmas (SH), ion beams (IBEAMS). The green box denotes the region of semiconductors (scaled with the excitonic a_B, E_R). Plasmas in traps (TR) are outside the figure, typically at sub-Kelvin temperatures.

Fig. 1 shows a qualitative phase diagram of Coulomb systems in equilibrium as a function of temperature and density. It allows to compare different Coulomb systems and projects results from one area onto another. One simply has to rescale length and energies in the actual a_B and E_R using the corresponding data for m, e, d and ϵ. As an illustrative example, Fig. 1 shows that the electron-hole plasma in semiconductors covers a remarkably broad range of situations in laboratory and space plasmas.

2 Coulomb Structures in Equilibrium

The general behavior is well known: in the limit of high temperature, $\chi \ll 1$ and $\Gamma \ll 1$, CS behave as a classical ideal gas of free charge carriers. Similarly, in the limit of high

densities, $\chi \gg 1$ and $r_s \ll 1$, ideal gas behavior is recovered, however, that of a quantum gas of spatially extended mutually penetrating particles. Both limits are structureless and comparatively simple theoretically: they are succesfully (and rigorously) treated by perturbation theory (with respect to Γ or r_s). Much more interesting behavior emerges when the Coulomb energy starts to exceed the kinetic energy, i.e. $\Gamma \geq 1$ or $r_s \geq 1$ – the behavior of charged particles is then strongly correlated, electrons may become trapped by ions leading to the formation of atoms, molecules and macroscopic matter. This parameter range is very challenging theoretically due to the absence of small expansion parameters. Traditional classical and quantum statistical methods, e.g. Ref. 5, 4, are able to describe only certain types of these correlations by summing special classes of diagrams (such as ladder type diagrams describing atoms or excitons).

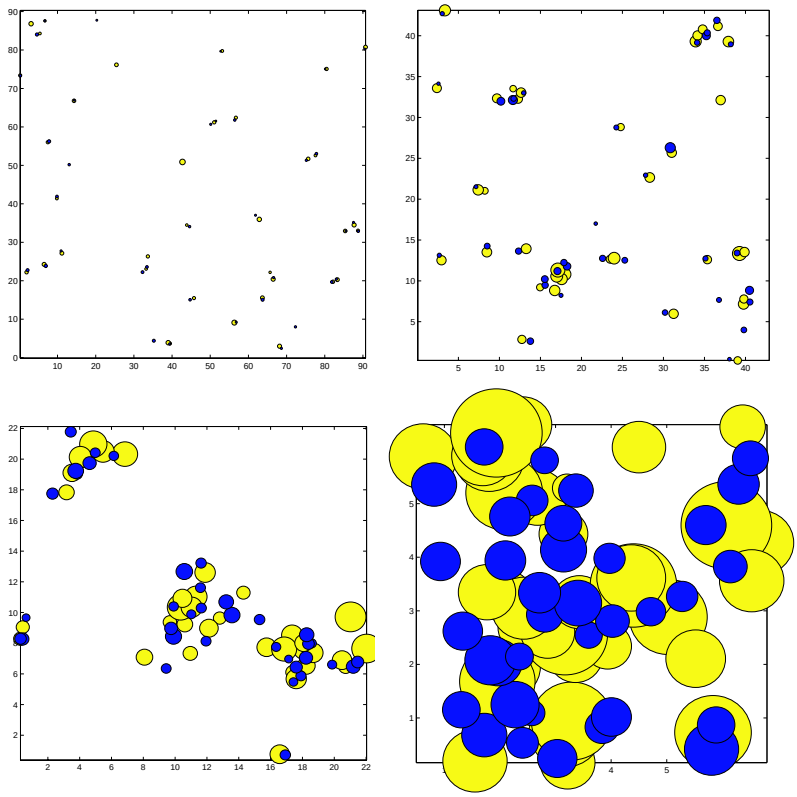

Figure 2. Snapshots of a correlated quantum electron-hole plasma in a two-dimensional semiconductor quantum well at low temperature $T = 0.1E_R$ simulated with path integral Monte Carlo. The densities are: $r_s = 8.6$ (top left), $r_s = 4.2$ (top right), $r_s = 2.1$ (bottom left) and $r_s = 0.6$ (bottom right). Yellow (blue) dots show the average quantum extension of an electron (hole).

The alternative here is first-principle simulations such as path integral Monte Carlo (PIMC) which do not have restrictions with respect to the coupling strengths, e.g. Ref. 6–8.

Fig. 2 shows direct fermionic PIMC simulations for an excited electron hole plasma in a semiconductor quantum well in the range of strong correlations. Both electrons and holes are strongly degenerate, i.e. $\chi_{e,h} > 1$, thus a quantum-mechanical treatment is essential. The PIMC simulations yield the correct size of the electrons and holes (the dots indicate the average extension of the wave function). If the density is increased (from the top left to the bottom right figure) this size becomes comparable to and even exceeds the mean interparticle distance width. The temperature is chosen well below the exciton binding energy, and formation of localized electron-hole pairs (excitons), three-particle complexes (trions), molecules (bi-excitons) is evident at low density (large r_s). With increasing density (bottom figures), even larger complexes form – electron-hole droplets which have been predicted by Keldysh more than 3 decades ago and observed experimentally.

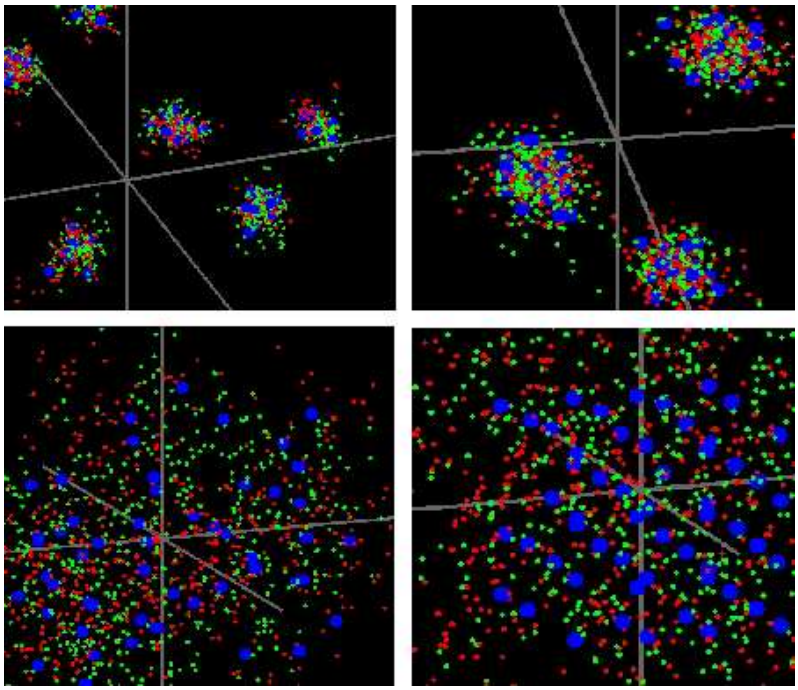

Figure 3. PIMC simulation snapshots of strongly correlated hydrogen plasma at $T = 10,000K$ in 3D space (gray lines are the coordinate axes). Electrons are shown by clouds of small dots, red and green dots denote electrons with different spin projections. The protons are treated classically and marked by large blue dots. Densities are: $n = 10^{22}\text{cm}^{-3}$ (top left figure), $n = 3 \cdot 10^{22}\text{cm}^{-3}$ (top right), 10^{24}cm^{-3} (bottom left) and 10^{26}cm^{-3} (bottom right). Scales on the axes are increased with density according to $\bar{r} \sim n^{-1/3}$.

Very similar situations exist in dense plasmas found in the interior of the giant planets, brown dwarf stars or in plasma compression experiments, cf. Fig. 1. Similarly, also the PIMC simulations can be directly applied to these systems, and results for dense hydrogen are shown in Fig. 3. Obviously, the main difference is the much larger mass ratio of ions and electrons compared to electron-hole systems, which allows to treat the ions classically

(i.e. as point-like particles, they are shown by blue dots in the figure). In contrast, the electrons are treated quantum-mechanically, fully including diffraction effects (finite extension, given by the size of the clouds of small dots) and fermionic exchange (red and green colors denote electrons with different spin projection). The peculiar feature shown in the top figures is the formation of large clusters which contain several protons embedded into de-localized electrons. This is very similar to the electron-hole droplets, cf. Fig. 2, and indicates an instability of the homogeneous plasma state at low temperature which may be related to the hypothetical plasma phase transition, e.g. Ref. 9, 10. As the density is increased further (bottom figures) the electron extension Λ exceeds the Bohr radius and bound states and clusters become unstable. The bottom left figure shows a high density liquid-like plasma state. Further increase of the density by two orders of magnitude leads to an unusual state where the electrons behave like a completely delocalized weakly interacting quantum gas ($\chi_e \gg 1, r_s \ll 1$), the protons, however, are still classical ($\chi_p < 1$) but so strongly coupled ($\Gamma > 175$) that they form a Wigner lattice embedded into the electron gas, see bottom right figure. Such behavior is expected to occur in high-density stellar objects, and it is very encouraging that PIMC simulations are able to correctly reproduce it. Still these simulations of fermions at high density are in their infancy which is due to the fermion sign problem, e.g. Ref. 7. A solution of this problem for strongly correlated Coulomb systems, either by appropriate additional approximations (restricted PIMC, e.g. Ref. 11) or direct simulations[12, 13, 7]), remains a major challenge in the theory of quantum Coulomb systems.

3 Nonequilibrium Theory of Correlated Coulomb Systems

A theoretical description of Coulomb systems starts from the Hamiltonian

$$\hat{H} = \hat{K} + \hat{U}_c + \hat{U}_{ext}, \quad \hat{K} = -\sum_{i=1}^{N} \frac{\hbar^2 \nabla_i^2}{2m_i}, \quad \hat{U}_c = \sum_{i<j}^{N} \frac{e_i e_j}{\epsilon |\vec{r}_i - \vec{r}_j|}, \tag{1}$$

where K, U_c and U_{ext} denote the kinetic energy, Coulomb interaction energy and energy due to external fields. Equilibrium theories are derived from the N-particle density operator $\hat{\rho}_N = e^{-\hat{H}/kT}$ which, for Fermi systems, has to be properly anti-symmetrized. Any observable can be computed from the density operator, e.g. Ref. 4, 3 by using quantum-statistical or simulation methods. In particular, PIMC methods are able to yield first-principle results of the equilibrium properties of CS. However, so far no comparably powerful method exists for time-dependent (dynamical, transport, optical) properties which require solution of the equation of motion of the density operator, the von Neumann equation,

$$i\hbar \frac{\partial}{\partial t} \hat{\rho}_N(t) - [\hat{H}, \hat{\rho}_N(t)] = 0. \tag{2}$$

An exception are classical Coulomb systems where Eq. (2) reduces to the equations of classical mechanics (Newton's equations) which can be integrated directly (molecular dynamics, MD). There exist various attempts to extend MD to *quantum* Coulomb systems three of which will be mentioned here. The first is the concept of wave packet MD[14] where one computes quasi-classical phase space trajectories of particles which are represented by

a wave packet of finite extension in coordinate and momentum space. A second approach is quasi-classical MD (QCMD) where one retains (in the dynamics) the point size of the particles but includes quantum effects into a modified interaction potential which takes into account quantum extension effects at small inter-particle distances, see Sec. 3.1 and Ref. 15. As a third approach we mention the Wigner function MD (WFMD) where Eq. (2) is transformed to the Wigner representation and solved directly for the N-particle density matrix $\rho(R_1, p_1, \ldots R_N, p_N)$, see e.g. Ref. 16.

Besides these particle-based methods there exist powerful quantum kinetic approaches[5,4,3]. There, the equation for ρ_N is transformed into a kinetic equation for the single-particle density operator $\rho_1 \equiv \mathrm{Tr}_{2\ldots N}\rho_N$, the one-particle Wigner function $f(R,p,t)$, or the one-particle Green's functions $G^{\gtrless}$. The latter are defined by

$$\begin{aligned} G^{<}(\mathbf{k}+\mathbf{q},t_1;\mathbf{k},t_2) &= i\langle a^{\dagger}_{\mathbf{k}}(t_2)a_{\mathbf{k}+\mathbf{q}}(t_1)\rangle; \\ G^{>}(\mathbf{k}+\mathbf{q},t_1;\mathbf{k},t_2) &= -i\langle a_{\mathbf{k}+\mathbf{q}}(t_1)a^{\dagger}_{\mathbf{k}}(t_2)\rangle, \end{aligned} \tag{3}$$

where the field operators $a_{\mathbf{k}+\mathbf{q}}(t_1)$ and $a^{\dagger}_{\mathbf{k}}(t_2)$ denote annihilation of a particle with momentum $\mathbf{k}+\mathbf{q}$ at time t_1 and creation of a particle with momentum $\mathbf{k}$ at time t_2, respectively which assure exact fulfillment of the Fermi statistics. The equations of motion for $G^{\gtrless}$ are the Kadanoff-Baym/Keldysh equations (KBE)[5,17],

$$\begin{aligned} \left(i\hbar\frac{\partial}{\partial t_1} - \epsilon_{\mathbf{k}_1}\right) G^{\gtrless}(\mathbf{k}_1 t_1;\mathbf{k}_2 t_2) - \sum_{\mathbf{q}} U_{ext}(-\mathbf{q},t_1) G^{\gtrless}(\mathbf{k}_1-\mathbf{q},t_1;\mathbf{k}_2 t_2) = \\ \sum_{\bar{\mathbf{k}}} \Sigma^{\mathrm{HF}}(\mathbf{k}_1 t_1;\bar{\mathbf{k}} t_1) G^{\gtrless}(\bar{\mathbf{k}} t_1;\mathbf{k}_2 t_2) + I^{\gtrless}(\mathbf{k}_1 t_1;\mathbf{k}_2 t_2), \end{aligned} \tag{4}$$

(to be supplemented with the adjoint equation), where Σ^{HF} is the Hartree–Fock selfenergy, and the collision integrals $I^{\gtrless}$ contain the short-range correlation effects (see below).

The advantage of these methods is that quantum and spin effects are built in rigorously. The problem, on the other hand, is the difficult (or inefficient) treatment of strong correlations, as in the equilibrium case. Here, it manifests itself in the familiar fact that the equations for f or $G^{\gtrless}$ are not closed but couple to the equations of motion for the two-particle function f_{12} or G_{12} and so on, giving rise to a hierarchy of equations (BBGKY-hierarchy of reduced density operators, e.g. Ref. 3 or Martin-Schwinger hierarchy of the Green's functions[5,4,3]). Solution of the kinetic equation requires decoupling of the hierarchy which is related to an approximate treatment of correlation effect. To solve Eq. (4), a formal closure is performed by introducing a selfenergy according to $\mathrm{Tr}_2 V_{12} G_{12} = \Sigma_1 G_1$. Below we show results where Σ_1 is used in the static Born approximation.

Finally, we point out that the KBE have several important advantages compared to convential kinetic equations (CKE, such as the Boltzmann, Landau or Vlasov equation): they *conserve total energy* (kinetic plus correlation energy[3,18,19]) whereas CKE conserve only kinetic energy, and they describe relaxation to a *correlated equilibrium* state whereas CKE always yield an ideal equilibrium (given by a Maxwell or Fermi/Bose distribution function). These properties are crucial in the description of relaxation processes in correlated Coulomb systems. Besides the KBE, these requirements are also fulfilled by classical MD simulations (with the problems in handling quantum and spin effects noted above).

3.1 Dynamical Properties. Plasmon Spectrum

As a first example of nonequilibrium properties of quantum Coulomb systems we consider dielectric properties. Oscillations of weakly correlated plasmas have been investigated in extraordinary detail during the last half century, the standard result for uncorrelated classical and quantum plasmas is given by the Vlasov approximation and random phase approximation (RPA), respectively. Similarly as for the equilibrium properties (Sec. 2), CS show also universal dynamical behavior: the long-range Coulomb interaction gives rise to a characteristic time scale, the plasma period $T_{pl} = 2\pi/\omega_{pl}$, where $\omega_{pl}^2 = 4\pi n e^2/(\epsilon m)$. ω_{pl} is the universal eigenfrequency of a macroscopic classical or quantum one-component plasma and is not affected by short-range correlations. On the other hand, correlation and quantum effects influence the frequency of plasma oscillations of finite range (finite wavenumber q), leading to a reduction of the frequency and to an increased damping. To compute these effects requires to go beyond the Vlasov and RPA level which has been proven difficult since a number of consistency requirements – most importantly sum rules – have to be fulfilled.

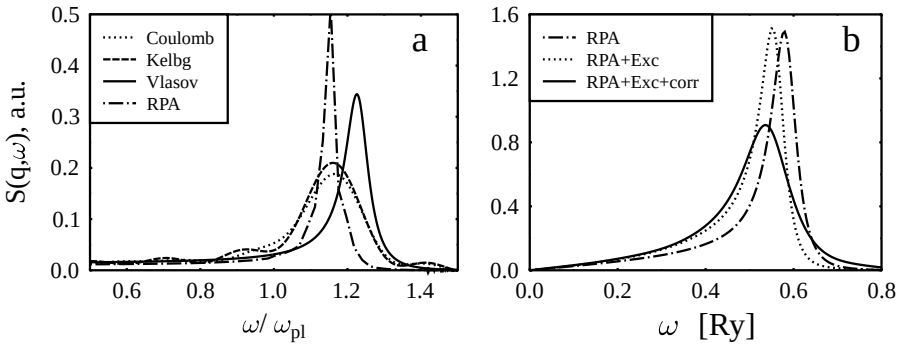

Figure 4. Dynamic structure factor of a correlated quantum electron gas for a fixed wave number. The figure compares standard models which neglect correlations (RPA and Vlasov) with two first principle simulations which conserve density and total energy: classical molecular dynamics (a) and quantum kinetic theory (b).

One approach that meets these requirements are quantum kinetic equations. It has been demonstrated that due to conservation of total energy (and density) the solution of the KBE (4) with a monochromatic external excitation $U_{ext} = U(t)\cos q_0 t$ includes the required set of correlation corrections (selfenergy and vertex terms) selfconsistently and guarantees sum rule preservation[5,17]. Fig. 4b shows, for a fixed wave number q_0, the result of correlations and fermionic exchange (full line) in comparison to the RPA[17]. The second approach capable to yield rigorous results for the plasmon spectrum of correlated CS is molecular dynamics, e.g. Ref. 20. Fig. 4a show results of classical MD with a quantum potential[15] – the Kelbg potential,

$$U_{\rm KELBG}(r,T) = 4\pi e^2 \left(\frac{1-\exp(-r^2/\lambda^2)}{r} + \frac{\sqrt{\pi}}{\lambda} {\rm erfc}(r/\lambda) \right), \qquad (5)$$

where $\lambda(T) = \Lambda/\sqrt{2\pi}$. $U_{\rm KELBG}$ correctly takes into account quantum diffraction effects (in particular it has a finite height at zero r) and, at large distances, approaches the Coulomb

potential. Fig. 4a shows that correlations lead to an additional damping of the plasmon (increased width of the peak) and a reduction of its energy thereby also preserving sum rules[15]. Further development of this QCMD approach and its extension to strong coupling and strong degeneracy are possible by derivation of improved quantum potentials[21].

3.2 Short-Time Dynamics. Plasma Cooling

Let us now consider rapid processes in correlated CS which proceed on the time scale of the plasma period T_{pl}. This is the time necessary to correlate the particles after the plasma is being created – the time to build up the pair distribution function, the plasmon spectrum and the screening cloud[18,3,22]. This build up of correlations among initially independent (uncorrelated) particles is shown in Fig. 5: The magnitude of Coulomb interaction (and kinetic) energy increases during a short initial period and remains constant for $t \gtrsim T_{pl}$.

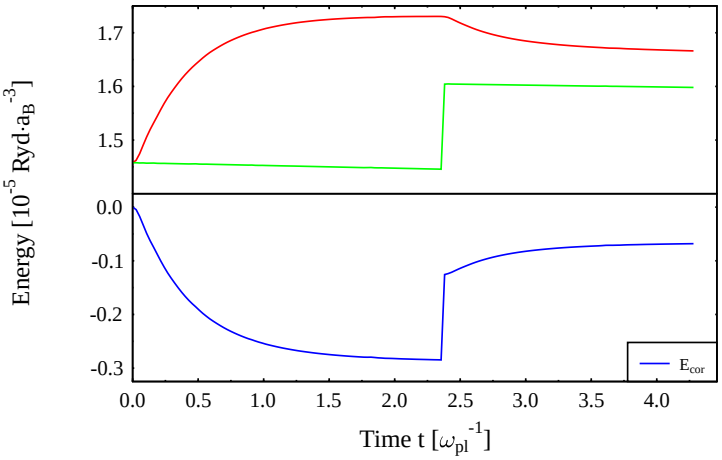

Figure 5. Energy relaxation in a one-component plasma before and after a sudden reduction of the interaction from solution of the KBE (4). Initially, correlations are being build-up, causing heating of the system. After reduction of the interaction correlations are being reduced, the plasma cools[24]. Blue (red) – correlation (kinetic) energy, green – total (kinetic plus correlation) energy.

Now it is interesting to ask if one can achieve the opposite: bring the plasma into a state which is *overcorrelated*[3,23]. As a consequence, the magnitude of correlation energy would be reduced leading to a reduction of kinetic energy, owing to total energy conservation. A possible realization is demonstrated in Fig. 5: at $t \approx 2.5/\omega_{pl}$ the interaction between the particles is reduced so rapidly that they have no time to readjust their arrangement. During a subsequent evolution lasting to about $t \approx 4/\omega_{pl}$ the plasma responds to this modification: pair correlations are weakened, leading to a reduction of the magnitude of correlation energy and of kinetic energy – the system cools. Such schemes are indeed possible[24], best candidates are two-component plasmas with large mass difference, such as ions in traps or dusty plasmas. For a theoretical description of these processes, again, models are needed

which conserve total energy and allow to describe fast changes in the system: generalized quantum (or classical) kinetic equations and molecular dynamics, more detailed results are given in Ref. 24.

4 Computational Aspects and Conclusion

In this paper, we have discussed correlated quantum Coulomb systems and approaches for a rigorous theoretical and computational treatment. Naturally, only a few concepts have been discussed in some detail which, nevertheless, characterize the present situation in the field: there exist powerful approaches each of which is capable for a first-principle description of certain limiting cases or certain particular properties of QCS[2]. Therefore, a very fruitful direction of research appears to be to find combination of these (and possibly other) theoretical and numerical methods.

The results presented in the first part of this paper are based on path integral Quantum Monte Carlo simulations. These simulations run very well on massively parallel computers (and we were lucky to use the CRAY T3E of the NIC Jülich). The parallelization is trivial and almost without communication bottleneck: each processor is given a different initial configuration and independently computes its own equilibrium state (the state of highest probability). After convergence is reached, macroscopic observables, such as total energy, equation of state or the pair distributions are obtained by averaging over the data of all processors.

Our nonequilibrium results are based on numerically solving quantum kinetic equations. Here the main CPU time consumption goes into evaluation of the collision integrals, i.e. the r.h.s. of Eqs. (4). These integrals are non-Markovian, i.e. involve a time integration over the whole history of the system. This situation is much less adapted to straightforward parallelization. Instead we found it advantageous to use the NIC's vector machine which allowed to effectively compute the integration loops (which were transformed into huge vectors over momenta and time arguments).

Acknowledgments

The authors devote this article to the memory of Prof. Wilfried Schäfer (Jülich) who deceased in August 2003. His continuous interest in our work was a great stimulus for us. The authors are grateful to the colleagues at NIC Jülich for providing us with CPU time on their parallel and vector computers and assistence in solving many technical problems. This work has been supported by the Deutsche Forschungsgemeinschaft (BO1366-2) and SFB 198 (B10), and by the Deutsche Physikalische Gesellschaft via the Gustav-Hertz-Prize.

References

1. M. Bonitz, Physik Journal July/August 2002, pp. 69-75 (in German).
2. The present lecture is based on the article by M. Bonitz, D. Semkat, A. Filinov, V. Golubnychiy, D. Kremp, D.O. Gericke, M.S. Murillo, V. Filinov, V. Fortov, W. Hoyer, and S.W. Koch., J.Phys.A.: Math. Gen. **36**, 5921 (2003), where also further references can be found.

3. M. Bonitz, *Quantum Kinetic Theory*, Teubner-Verlag, Stuttgart/Leipzig 1998.
4. W.D. Kraeft, D. Kremp, W. Ebeling, and G. Röpke, *Quantum Statistics of Charged Particle Systems*, Akademie-Verlag Berlin 1986.
5. L.P. Kadanoff and G. Baym, *Quantum Statistical Mechanics*, Addison-Wesley Publ. Co. Inc., 2nd ed., 1989.
6. B. Militzer, and D.M. Ceperley, Phys. Rev. Lett. **85**, 1890 (2000).
7. V.S. Filinov, M. Bonitz, W. Ebeling, and V.E. Fortov, Plasma Phys. Contr. Fusion **43**, 743 (2001).
8. A. Filinov, M. Bonitz, and Yu. Lozovik, Phys. Rev. Lett. **86**, 3851 (2001).
9. M. Schlanges, M. Bonitz, and A. Tschttschjan, Contrib. Plasma Phys. **35**, 109 (1995).
10. V.S. Filinov, V.E. Fortov, M. Bonitz, and P.R. Levashov, JETP Lett. **74**, 384 (2001) [Pis'ma v ZhETF **74**, 422 (2001)].
11. B. Militzer, and E.L. Pollock, Phys. Rev. E **61**, 3470 (2000).
12. V.S. Filinov, M. Bonitz, and V.E. Fortov, JETP Letters **72**, 245 (2000).
13. V.S. Filinov, V.E. Fortov, M. Bonitz, and D. Kremp, Phys. Lett. **A 274**, 228 (2000).
14. H. Feldmeier, and J. Schnack, Rev. Mod. Phys. **72**, 655 (2000).
15. V. Golubnychyi, M. Bonitz, D. Kremp and M. Schlanges, Phys. Rev. E **64**, 016409 (2001).
16. V.S. Filinov et al., Phys. Rev. B **65**, 165124 (2002) and references therein.
17. N.H. Kwong and M. Bonitz, Phys. Rev. Lett. **84**, 1768 (2000).
18. M. Bonitz et al., J. Phys. B: Cond. Matt. **8**, 6057 (1996).
19. D. Kremp, Th. Bornath, M. Schlanges, and M. Bonitz, Phys. Rev. E **60**, 4725 (1999).
20. J.P. Hansen, Phys. Rev. **A**, 3096 (1973).
21. A. Filinov, M. Bonitz, and W. Ebeling, J.Phys.A.: Math. Gen. **36**, 5899 (2003).
22. For an experimental demonstration in semiconductors, see R. Huber, F. Tauser, A. Brodschelm, M. Bichler, G. Abstreiter, and A. Leitenstorfer, Nature **414**, 286 (2001).
23. D. Semkat, D. Kremp, and M. Bonitz, J. Math. Phys. **41**, 7458 (2000).
24. D.O. Gericke, M.S. Murillo, D. Semkat, M. Bonitz, and D. Kremp, J.Phys.A.: Math. Gen. **36**, 6087 (2003).